TITLE

A Shape Analysis Algorithm Quantifies Spatial Morphology and Context of 2D to 3D Cell Culture for Correlating Novel Phenotypes with Treatment Resistance

AUTHORS AND AFFILIATIONS

David H. Nguyen, Ph.D., Tissue Spatial Geometrics Laboratory, Concord, CA, USA

SUMMARY

This article explains how novel features of morphology in cells and organoids can be measured by the Linearized Compressed Polar Coordinates (LCPC) Transform, a spatial algorithm that measures what traditional metrics, such as area, volume, surface area, etc., cannot. Best practices for shape orientation and alignment are discussed.

ABSTRACT

Numerous studies have shown that the morphological phenotype of a cell or organoid correlates with its susceptibility to anti-cancer agents. However, traditional methods of measuring phenotype rely on spatial metrics such as area, volume, perimeter, and signal intensity, which work but are limited. These approaches cannot measure many crucial features of spatial context, such as chirality, which is the property of having left- and right-handedness. Volume cannot register chirality because the left shoe and right shoe hold the harbor the same amount of volume. Though spatial context in the form of chirality, direction of gravity, and the axis of polarity are intuitive notions to humans, traditional metrics relied on by cell biologists, pathologists, radiologists, and machine learning scientists up to this point cannot register these fundamental notions. The Linearized Compressed Polar Coordinates (LCPC) Transform is a novel algorithm that can capture spatial context unlike any other metric. The LCPC Transform translates a two-dimensional (2D) contour into a discrete sinusoid wave via overlaying a grid system that tracks points of intersection between the contour and the grid lines. It turns the contour into a series of sequential pairs of discrete coordinates, with the independent coordinate (x-coordinate) being consecutive positions in 2D space. Each dependent coordinate (y-coordinate) consists of the distance, between an intersection of the contour and gridline, to the origin of the grid system. In the form of a discrete sinusoid wave, the Fast Fourier Transform is then applied to the data. In this way, the shape of cells in 2D and 3D cell culture, are represented systematically and multidimensionally, allowing for robust quantitative stratification that will reveal insights into treatment resistance.

INTRODUCTION

Three-dimensional (3D) organoid culture has proven superior to two-dimensional (2D) cell culture in mimicking *in vivo* biology (Masako, 2020; Abbas, 2023). Organoids have become indispensable in cancer research for the purposes of screening for effective treatments and extracting insights into disease progression. While it is plain knowledge in the field of cancer biology that distinctions in morphology correlate with the distinct biological behavior of cells and tissues, the field relies on traditional shape metrics that are limited in their scope. This study describes a novel spatial algorithm that objectively quantifies subtle features of morphology in unprecedented precision compared to traditional approaches of area, volume, surface area, etc.

Numerous studies have shown a correlation between tumor organoid morphology and treatment resistance. Patient-derived colorectal cancer organoids exhibit distinct 3D morphologies, such as solid structure, cystic structure, and budding morphology, which correlate with sensitivity or resistance to drug therapies (Betge, 2022). Furthermore, colon cancer organoids derived from patients that were either sensitive or resistant to oxaliplatin chemotherapy exhibited distinct morphologies. Resistant organoids that underwent genetic knockout of the long non-coding RNA lnc-RP11-536 K7.3 become sensitive to oxaliplatin, but the surviving organoids exhibited a morphology that was distinct from that at the start of treatment (Li, 2021). Hadj Bachir et al. (2022) developed tumor organoids from Pancreatic Ductal Adenocarcinoma that were resistant to FOLFIRINOX treatment. Compared to organoids that were sensitive to treatment, when the resistant organoids reached developmental maturity and exhibited folding patterns, their folding was more complex than those observed in the sensitive organoids, highlighting clear morphological differences associated with chemoresistance. Masako et al. (2020) studied thirteen triple negative breast cancer cell lines and found that those what grew in 3D as spheroids were more resistant to chemotherapy than those described as grape-like. Zhao et al. (2021) showed that certain mesenchymal mammary tumor organoids exhibited a spikey morphology, which changes to a jagged edge morphology upon induction of miR-200c, a micro-RNA that induces mesenchymal-to-epithelial (MET) transition. Based on this distinct phenotypic change, the authors developed a morphology-based screening method to identify drugs that can induce MET and thereby enhance chemosensitivity.

While there is ample evidence across multiple types of cancer, beyond the studies cited here, that organoid morphology is indicative of treatment resistance, studies up to this point rely on metrics such as diameter, area, volume, and surface area. The existence of automated high-throughput cell culturing techniques that include imaging components means that morphology data is accessible as part of the research and development pipeline. However, without methods that robustly quantify subtle differences in morphology, it is difficult to discover unknown morphological subtypes and/or leverage the power of machine learning to correlate these subtypes with disease progression and treatment resistance.

The Importance of Spatial Context for Biological Morphology

Biology and nature are full of spatial contexts that are crucial to proper function. Epithelial cells have inherent morphological spatial context, such as apical-basal polarity, to execute their

function of forming barriers and directionally secreting products (Roignot, 2013; Tharp & Weaver, 2018; Campanale, 2017; Martin, 2021). When cells migrate 2D cell culture, the leading edge of the cell has a distinct morphology compared to the trailing edge. This asymmetry in cell morphology during migration is essential for sensing the environment and for anchoring the cell for generating force in specific directions.

Another crucial spatial context in nature is the direction of gravity. Bone health, muscle health, and vascular health in astronauts become dysfunctional due to prolonged exposure to microgravity conditions (Khune, 2024; Tomsia, 2024). Not surprisingly, cancer cells behave very differently in microgravity compared to being on Earth, including alterations in their morphology as single cells and in 3D colonies (Kim, 2024; Grimm, 2025; Yuan, 2026).

A third spatial context in cancer is that in situ pre-neoplasia and neoplasia can sprout from a base, or trunk, which is its central support structure. Pedunculated colon polyps are an example of this morphology. As the lesion regresses, it changes shape towards this central support structure, which is also its bridge to the stable vascular network that carries oxygen (Ciocalteu, 2018; Teo, 2020).

The Limits of Traditional Shape Metrics

Traditional shape metrics used in cancer research and cell biology include measuring area, surface area, volume, perimeter, etc. While these metrics are informative, they cannot register spatial contexts that are obvious to humans. The apical-basal polarity of a cell in a lumen, the direction of gravity, and the direction of the central support structure is non-existent to traditional approaches that cannot register spatial context.

Traditional metrics also cannot distinguish gradations of shape change between common shape concepts, such as a square that is standing on one of its flat sides and a diamond that is the same square but rotated so that it stands vertically on one corner. Any intermediate forms resulting from rotating the square about its center to become the diamond are subjective interpretations. Are the intermediate steps “rotated squares” or “rotated diamonds”? Measuring area and perimeter to answer this question is pointless because the square and diamond equivalent by these two metrics. Another shortcoming of traditional shape metrics is that they cannot distinguish between size and shape. A series of circles that gradually increase in size will exhibit increasing area and perimeter measures, even though the shape concept never changes, meaning the circles remain circles.

A Novel Algorithm and Its Clever Augmentations Can Register Spatial Context

This study presents the Linearized Compressed Polar Coordinates (LCPC) Transform that was invented with the intention of objectively and quantitatively describing complex morphologies observed in tissue histopathology for the purposes of enhancing the grading of colon polyps. The desire to then expand this approach to capture spatial features in brain pathologies, such as Bipolar Disorder and Alzheimer’s Disease led to augmentations that enhanced it even further, which are described herein.

Open-source Python scripts have been developed and made publicly available, including scripts that do pre-processing steps such as contour extractions and rotations. This study describes the step-by-step protocol and best practices for applying two versions of LCPC Transform: the parallel grid system and the radial grid system. Advice is provided on when to

use which system for obtaining optimal results. The GitHub repository containing the scripts includes multiple sets of practice images and their results, so that users can replicate the results to ensure that the scripts are working as intended.

The LCPC Transform provides an unprecedented level of precision in measuring spatial information because it represents shapes in multiple dimensions. Unlike traditional methods, like area and volume, which yield only one scalar value per shape (i.e. 25 cm^2), the results of the LCPC Transform can yield multiple indices, each correlating with a different morphological aspect of a shape (i.e. roundness vs. sharpness of corners, smoothness vs. jaggedness of edges). The LCPC Transform is poised to revolutionize shape analysis for many fields of science, allowing users to measure what might be sub-dimensions of spatial information in between the x-, y-, and z-dimensions. It is now possible to measure what is hidden to the naked eye and to the traditional approaches derived from classical geometry. Like the Ancient Greek mathematician Archimedes who realized that the volume of water displaced by an object is also a measure of the object's density, this study describes a "Eureka" moment that will allow humans to measure nature in whole new ways.

PROTOCOL

How Does the LCPC Transform Work?

The LCPC Transform describes a 2D shape by overlaying a grid system of straight lines that intersect with the contour of the shape. Each grid system has an origin (Figure 1A) or a baseline (Figure 2A) from which to measure linear distance. Every point of intersection between the gridlines and the contour of the shape is detected. The distance of each intersection is then calculated relative to a baseline or origin. In this way, the LCPC Transform converts 2D shapes into a series of consecutive x and y pairs of coordinates. The x-coordinate represents the position of the gridline from zero to infinity, while the y-coordinate represents the distance of the intersection to the baseline or origin. In this form, which is a discrete sinusoid wave, the Fast Fourier Transform (FFT) is then applied to convert the data from the "position domain" to the frequency domain. If the x-coordinate represented time, then the "position domain" would be equivalent to the "time domain" in the standard applications of the FFT.

While the radial grid system measures the distance of each intersection from the origin of the radial grid (Figure 1A), the parallel grid system always measures the distance of intersections with reference to an imaginary line at the left of the shape (Figure 2A). The open-source script determines the position of this imaginary line by finding the left-most pixel of the contour and then moving 10 pixels to the left of this position. Here, the x-coordinate of this position becomes the reference point from which all intersections are calculated. This 10-pixel rule is arbitrary but is why all contours analyzed by the open-source script for the parallel grid system must have at least 15 pixels of white space on all four sides of a contour.

For 2D shapes that have folds or multiple layers, gridlines may intersect with the contour more than once. In this case, the distances of all intersections on a gridline are summed into one value. Thus, each gridline has only one x-coordinate and one y-coordinate. This summation is represented by the term "compressed" in the name of LCPC Transform. The rendering of a non-linear 2D shape into a discrete sinusoid wave is represented by the term "linearized" in the

algorithm's name. Lastly, the term "polar coordinates" is in the algorithm's name was because the first grid system conceptualized was a 180-degree radial grid of polar coordinates (Nguyen, 2018). Even after the realization that polar coordinates and Cartesian coordinates are interchangeable, the name of the algorithm was kept as is. The acknowledgements section describes the personal reasons that motivated the invention and augmentation of the LCPC Transform.

The frequency domain of the LCPC Transform reveals objective and quantitative features of a 2D shape that the naked eye cannot readily perceive. Very subtle differences in curvature, jaggedness, and tortuosity can be robustly quantified. However, once morphological subtypes are identified via this method, visually distinct themes can be observed that correlate with the quantitative differences. This feature makes the LCPC Transform interpretable as a method of extracting spatial information for machine learning (ML) models and makes the resulting ML models themselves more interpretable. While neural networks are a powerful ML method, their results are often not interpretable to humans, which is a significant problem for the field of medical artificial intelligence (AI). Physicians are reluctant to employ an ML model for clinical decisions if they don't understand why the model makes bad decisions. Furthermore, if no human understands why or how a model made a biased decision, then fixing this becomes intractable.

This manuscript describes only two grid systems for the LCPC Transform, though many grid systems exist. It is important to note that though all grid systems can extract spatial information, some will provide cleaner data than others. Thus, users are encouraged to apply both the parallel and the radial grid systems to their data to determine optimal fit. For simplicity and reproducibility, the open-source Python scripts only include a 360-degree radial grid system (Nguyen, 2025a) and a parallel grid system (Nguyen, 2025b), which will suffice for most applications. Again, all grid systems can extract spatial information, but some are better than others depending on the spatial contexts described in this manuscript. The aforementioned GitHub repositories contain links to YouTube videos that are tutorials on how to run the scripts on the associated practice images and how to do quality control checks on the outputs. It is highly recommended that users learn how and where to do quality control checks.

The Radial Grid System vs. The Parallel Grid System

In general, the radial grid system (Figure 1B) is good for shapes that radially symmetric, round, and closed. However, it also works well for shapes that are open (meaning the contour has at least one disconnected region) but curved in on itself (like the letter "c"). This grid system also works for contours that consist of multiple layers or even contours that have multiple non-intersecting components.

The parallel grid system (Figure 2B), on the other hand, is good for shapes that are elongated and open. Though it was previously stated that the radial grid system works well for closed shapes, closed shapes that are elongated sometimes yield cleaner results when assessed by the parallel grid system. Just as with the radial grid system, the parallel grid system can measure the spatial information of objects that consist of multiple non-intersecting components.

Importance of Standardizing Shape Orientation Prior to the LCPC Transform

As discussed in the introduction, nature is inherently polar, which includes the shapes of cells and organoids. Cells can have apical-basal polarity and organoids can have asymmetries that indicate poles. Thus, orienting shapes in a systematic and objective manner before extracting spatial information via the LCPC Transform will yield cleaner, more reproducible results. Figure 3A shows two shapes that are identical but mirror images of each other. Though they are the same shapes, because the parallel grid system always measures distances of intersections from the left side of the image, the parallel grid LCPC will yield different numbers for each image. The LCPC Transform was designed to capture spatial context, so it is very sensitive to seemingly minor differences in spatial context. A better way to compare Shape 2 to Shape 1 in Figure 3 is to flip Shape 2 horizontally, which changes the spatial orientation but doesn't change the shape, and then apply the parallel grid LCPC (as shown in Figure 3B).

Compared to traditional shape metrics, such as area, volume, and perimeter, that are not affected by spatial orientation, the LCPC Transform requires the user to think about how shapes should be oriented before measurement so that the optimal results are produced. The volume of liquid in an unopened can of soda does not change depending on whether the can is right-side up, upside down, or any other orientation.

When measuring shapes with the LCPC Transform, it is helpful to determine if the shapes should be re-oriented in a systematic way beforehand. Figure 3C shows four items that are shaped like the number "3" and arranged haphazardly. Unless there is a reason to keep each shape in its original orientation, the user should orient each shape like in Figure 3D. The rules for systematically aligning all items in Figure 3C into Figure 3D are: (1) The object is rotated such that the line that connects the opening of the "3" is vertical, (2) the wider part is on top, (3) and all objects have their concavity facing to the left so that the bulge of "3" pushes away from the left of the object where the parallel grid LCPC will place the reference baseline for measuring distance. Note that these rules require that Item 1 and Item 4 be both rotated and flipped horizontally, while Item 2 and Item 3 only need rotation. Flipping horizontally changes the spatial orientation of a shape, but not necessarily the shape. The user needs to determine what orientation rules to apply, and why, to every object, which will dramatically improve the cleanliness, and thus reproducibility, of the data.

It is important to note that the LCPC Transform can be applied to sub-compartments of a shape instead of the whole shape. Morphologies in nature are highly complex, so scientists often assume insignificance to minor features of morphology to simplify the system being studied. However, the LCPC Transform is revealing that seemingly minor differences in morphology can be quantitatively measured and correlated with distinct biological function. Thus, Figure 3E shows how the wider bulge of the items in Figure 3C can be extracted and objectively compared. However, Figure 3F shows how the user can compare these wider bulges in the context of the alignment rules in Figure 3D. Figure 3F and 3D are meant to highlight the fact that the user must determine what spatial context is relevant and why.

The Parallel Grid System for Measuring Density or Texture as an Index of Spatial Information

Spatial information involves more than the usual notions of shape, such as squareness, roundness, and curvature, because it encompasses concepts such as texture and density. Complex tubular networks, such as blood vessels, or branching networks, such as cytoskeletal

filaments, do not fit the notion of shape in the same sense of our geometry-based intuition on shapes, such as circles and squares. However, density and texture are very useful notions of spatial information for understanding the structure and function of cells and organoids. In dealing with how to quantify complex networks in fluorescence imaging, cell biologists measuring features such as the average signal intensity within an image or the percent of the total area of an image that contains a signal. These approaches recognize that there is more to spatial information than just describing it in terms of convenient geometry motifs.

For quantifying dense networks of tubes, islands, and branches, the parallel grid system is useful for measuring what can be called texture-density, instead of shape. As an example of how the parallel grid LCPC Transform can do this, Figure 4A shows cardiac microvasculature patterns from Gkontra et al. (2018): to the naked eye, objectively and quantitatively distinguishing the patterns between the infarcted area and the areas at a region remote from the site in injury is very difficult. By extracting the mask of the blood vessels (Figure 4B) and applying the parallel grid LCPC Transform, quantitative differences can be observed. To enhance the cleanliness of the data, each mask image was rotated such that the general axis of vessel alignment (Figure 4A, green line) is vertical. Furthermore, the edges of the masks were trimmed to be a uniform circle to remove differences due to lost corners because of rotation (Figure 4C). Analyzing the results via Principal Component Analysis (PCA) and plotting the first three principal components reveals that the infarcted regions cluster separately from the remote regions (Figure 4D). PCA is able to show distinct clustering patterns because the results of the parallel grid LCPC have certain frequency bins that show distinct differences between infarcted vs. remote tissue (Figure 4E). As a reference for the robustness of the LCPC Transform, a traditional metric of percent area covered by blood vessels is shown in Figure 4F. These results suggest that the parallel grid LCPC Transform can detect objective, quantitative differences in complex networks and textures that the naked eye and traditional methods cannot.

Deriving Informative Indices from Results of the Fast Fourier Transform

Though this manuscript refers to the LCPC Transform as including the step of applying the FFT, the actual LCPC Transform happens before FFT step (Figure 1A Step 4, Figure 2A Step 3). However, the effect of applying the FFT is to reveal objective, systematic insights from the frequency domain of the output of the LCPC Transform. Thus, the LCPC Transform would not be as effective without including the FFT as the final step.

In the LCPC Transform, the FFT results in a series of bins and their magnitudes, all of which are a static multidimensional representation of the contour inputted in step 1. An analogy of a static multidimensional representation of information is the nine-digit phone number representing a person's telephone communication channel in the United States. While cumbersome in comparison to scalar value representations of shapes (such as 85 cm in length, 56 degrees wide, etc.), multidimensional data harbors much more information for extracting insights.

The typical result of the LCPC Transform, including the last FFT step, is a histogram of magnitudes as a function of position (Figure 1A Step 5). The first bin has the largest magnitude, and subsequent bins can exhibit various repeating patterns. Figure 5 displays several hypothetical FFT results that have been observed. Each shape analyzed by the LCPC Transform

results in many frequency bins and their magnitudes that represent it, so using an unsupervised dimension reduction technique, such as Principal Component Analysis, is useful for exploring which bins are responsible for stratifying the experiment groups most. However, a complementary approach is to derive a single-valued scalar index from the FFT results to represent each shape. These indices allow for the ease of calculating statistical significance between experimental groups. The also allow for multiple distinct indices to be derived from the same FFT output, each representing different morphological features in the shapes being analyzed. This ability to provide multiple indices that each represent a different feature of morphology is unprecedented compared to traditional metrics, such as measuring the area within an object, which provides no more than one value for area. Figure 5A-5C show common patterns in bin magnitudes that can be used to create indices in the form of ratios. Figure 5A shows that there are three indices that can be derived based on the patterns highlighted by the dotted lines. Figure 5D shows hypothetical shape features that can correlate with different indices derived from the same FFT profile.

What is Pure Shape vs. At-Scale Shape?

One of the limitations of traditional shape metrics, such as area and perimeter, is that they measure both the shape of an object and the size of an object simultaneously and inextricably. Figure 6A shows a series of check mark-shaped objects that increase in size but are the same shape concept. While the area and perimeter of each check mark increase, the shape concept stays the same, but this is undetectable by area or perimeter. Figure 6B shows the concept of a square that becomes a diamond if it is rotated by 45 degrees. However, for any rotation between 0 and 45 degrees, the shape concept can be subjectively interpreted as either a “tilted square” or a “tilted diamond”. Through this series of rotations, the area and perimeter of each object don’t change while the shape concept does. The examples in Figure 6A and 6B highlight the inability of traditional shape metrics, such as area, volume, perimeter, and surface area in capturing notions that are obvious to humans.

When measuring shapes, the LCPC Transform can separate the effect of size from the effect of shape. In combination with an objective and systematic method of resizing objects, the LCPC Transform can measure what will be called “pure shape”, which is shape without the effect of size. Figure 7 shows two objects that are different in both shape and size. If they are not resized before being measured by the LCPC Transform, then they are being compared “at-scale”, meaning at their original scales relative to each other. However, by applying an objective set of rules for rotation and resizing, the two objects can be transformed to a similar scale while keeping their original shape. Figure 7 Step 2 shows how the longest internal line of each object is an objective morphological landmark by which the object can be rotated such that this line is horizontal. Step 3 of Figure 7 then shows how the width of both objects can be resized to be 400-pixels wide while also constraining the aspect ratio so that the object is not skewed (not constraining the aspect ratio while resizing a square turns it into a rectangle). In this way, both objects now have the same width. 400-pixels wide is an arbitrary value written into the open-source script. Lastly, Step 4 of Figure 7 shows an optional step of rotating the longest internal line with each object to be vertical, such that they get optimal coverage from the parallel grid LCPC Transform. If the radial grid LCPC Transform were applied, then this last rotation is unnecessary. However, it is suggested that the longest axis of objects be made vertical in case

the user wants to also apply the parallel grid LCPC Transform on the same objects for comparison with results the radial grid LCPC Transform. In the vertical position, the parallel grid LCPC Transform applies the greatest coverage across the object because the parallel lines are stacked vertically.

The step-by-step method for extracting the pure shape of objects described here has individual Python scripts that are available in the GitHub repository called “Pre-Processing-Tools-for-LCPC-Transform” (Nguyen, 2025c). Here is an example of the pre-processing steps to derive pure shape in preparation for the LCPC Transform. It is important to note that the scripts for doing either the radial grid or parallel grid LCPC Transform require that the masks of objects be blue lines on a white background. The color blue is arbitrary but assumed by the open-source scripts.

1. Crop each image to have a 1-pixel margin on all four sides of the blue object.
    - Script Name: “Trim margin to 1-pixel border.ipynb”
2. Add 100 pixels of white space on all four sides to create new margins.
    - This centers the object in the canvas and ensures that there are at least 15 pixels of white space on all four sides, which is a requirement for the LCPC Transform scripts. This step also allows for subsequent rotation steps to not cause the object to be cut-off due to rotations, which is a common problem when rotating an elongated object about its center. Script Name: “Add 100 pixels to margins.ipynb”
3. Rotate the objects such that the longest internal length is horizontal.
    - This step turns the longest internal line with each object into the object’s width. There are two scripts available for this purpose. For closed shapes, use Script Name: “Rotate CLOSED Object Horizontal by Longest Internal Length_v2.ipynb”. For open shapes or shapes with multiple components, use Script Name: “Rotate Green Line_v3.ipynb”
4. Crop each image to have a 1-pixel margin on all four sides of the blue object.
    - This is the same as Step 1. The purpose of trimming this time, however, is because the resizing step that comes next resizes the entire canvas, not just the blue object in it. Thus, by making the blue object nearly the same width and height as the canvas itself, resizing the canvas to 400-pixels wide also resizes the object to be nearly 400-pixels wide. Script Name: “Trim margin to 1-pixel border.ipynb”
5. Resize the canvas width of each image to be 400-pixels wide while also constraining the aspect ratio.
    - This step makes each object have the same width. Constraining aspect ratio prevents skewing the object during the resizing. Script Name: “Resize width to 400 pixels but constrain aspect ratio.ipynb”
6. Add 100 pixels of white space on all four sides to create new margins.

- This is the same as Step 2 and ensures that there are at least 15 pixels of white space on all four sides. Script Name: “Add 100 pixels to margins.ipynb”

7. Rotate each image either 90-degrees clockwise or counterclockwise to make the longest internal length vertical, being consistent with the choice for all images.
   - This step prepares the shapes to be optimally covered by the parallel grid LCPC Transform, while having no effect on the radial grid LCPC Transform. Script Name: “Rotate images 90CW.ipynb”, “Rotate images 90CCW.ipynb”

In the above sequence, pure shape is obtained by consecutively implementing Steps 3, 4 and 5. Adding margin space in Step 6 is required to avoid errors in the LCPC Transform scripts that will be done later but is not involved in extracting pure shape.

Users who desire to measure shapes “at-scale” need not perform Steps 3, 4, and 5 in the above protocol, though they should still pre-process their mask images to attain optimal orientation prior to applying the LCPC Transform.

The GitHub repository discussed above also contains scripts that are useful in pre-processing mask images. These include Python scripts for:

(1) flipping images into their mirror image (“Flip images VERTically.ipynb”, “Flip images HORIZontally.ipynb”),

(2) isolating multiple non-touching blue objects on a white canvas each onto their own white canvas so that each can be analyzed separately (“Isolate Objects Empty Blue.ipynb”),

(3) thickening the blue lines on a white background to attain optimal thickness, which is 5-10 pixels thick (“Thicken Blue Lines.ipynb”),

(4) for extracting colors from an image and turning those colors into a blue lines on a white canvas. There are five scripts, for extracting four color choices: red, green, blue, magenta. The purpose of these color extraction scripts is so that the user can manually or computationally segment neighboring shapes in an image using just one color or four distinct colors using any image editing software. Then, the user can use these scripts to extract all objects of the same color simultaneously to create blue contours of the segmented objects on a white background (“RED_Color Extraction (Mac).ipynb”, “BLUE_Color Extraction.ipynb”, “PINK_Color Extraction.ipynb”, “GREEN_Color Extraction.ipynb”, “RED_Color Extraction (Windows).ipynb”).

It is important to note that there are many image-editing software available outside of the provided Python scripts. Users can write their own scripts or use a preferred image-editing software to attain the same pre-processing results.

Adding Markers to Capture Spatial Orientation in Nature

Because traditional metrics, such as area, volume, and surface area, are agnostic to spatial context such as the direction of gravity, the direction of the strongest sunlight, and the axis of polarity, the LCPC Transform provides a unique opportunity to insert spatial markers that capture these contexts. As describe previously, how one rotates and orients a shape can also capture spatial context. Figure 8A shows another example of this in the form of cell migration in 2D culture. Figure 8B, however, is an example of how adding rationally placed information to the mask image allows the LCPC Transform to capture spatial context in exquisite ways. Figure

8B shows a hypothetical tumor or pre-cancerous lesion that is anchored outside of its encasement. The lesion grows or regresses within the encasement, while the encasement does not change. Thus, as the lesion grows away from, or regresses back to, its anchor due to therapeutic treatment, it does so relative to an encasement that remains static. This means that measures of area, perimeter, and volume (if the imaging context is 3D) would completely miss the fact that the spatial change in the lesion is happening within the context of an encasement. Why is this significant? In disease progression, the shape of cells, tissues, and organs do not change uniformly on all sides. They often grow away from or shrivel towards their central support structure. Furthermore, the "empty" space that they create relative to their encasement can have biological significance. Traditional shape metrics cannot capture the change of this "empty" space. Figure 8C shows two options for applying the parallel grid LCPC Transform to the contour of the lesions. The orange line in Figure 8B represents the location of the encasement directly across from the leading edge of the lesion. Including this orange line in the mask of the lesion, as shown in Figure 8C, captures the fact that there is significantly more empty space between Specimen 1 and its encasement than for Specimen 2 and its encasement. The dotted lines in Figure 8B represent an objective and rational manner to include the spatial context of the encasement without adding too little or too much extra information.

Notes on Statistical Methods

When doing PCA on a data from the LCPC Transform, the data should first be median-centered instead of mean-centered, because the LCPC Transform always results in a wide range of magnitudes and thus have what seem to be outliers. Bins 1, 2, and 3 are usually much greater in magnitude than the rest of the bins. However, the frequency domain typically produces data like this, so labeling extreme values as outliers is incorrect. Nonetheless, proper usage of PCA on data produced by the LCPC Transform requires an awareness of the wide data scatter resulting from the FFT.

Organoid volume was approximated by assuming a depth of 10 pixels between each slice, multiplying the area of each slice by this depth, and summing the results. Organoid surface area was approximated via the Trapezoidal Integration Method assuming a slice dept of 10 pixels. All calculations and statistical methods were done via standard Python libraries.

RESULTS

The Radial Grid LCPC Transform Applied to Consecutive 2D Slices of 3D Organoids

3D organoids and tumors can adopt a variety of shapes, some of which are obviously different to the human eye even though traditional metrics yield statistically insignificant differences. Figure 9A shows consecutive 2D slices of two hypothetical 3D organoids, one of which is shaped like a "pear" and the other a rounded-square. When the radial grid LCPC Transform is applied to each slice in its "natural", presented orientation in the figure the FFT results exhibited differences in relationship between Bin 3 and Bin 4 for the pear vs. the rounded-square. The ratio of Bin 3 to Bin 4 creates an index that exhibits a six-fold difference between the two organoids (Figure 9D). Summing this index for all slices in each organoid results in an average value by which to compare the two. The fold-change of the average value

between the two organoids shows that the rounded-square organoid is 1.77 times lesser than the pear organoid. The difference in averages does not reach statistical significance only because of one outlier in each organoid. The first slices, called Slice A in the Figure 9, in both organoids are the outliers. Slice A is the most distinct in terms of both size and shape compared to its groupmates. An enlarged view of Slice A for each organoid is shown in Figure 9E, highlighting the level of precision provided by the LCPC Transform. As a reference, the approximated volume and surface area of the two organoids is shown in Figure 9F, with only a 1.19-fold difference in volume and a 1.002-fold difference in surface area.

Note that the volume data shows that the Organoid 2 is larger than Organoid 1 even though the summed index values of Bin3/Bin4 in Figure 9E, derived from the LCPC Transform, shows the opposite effect. This highlights the fact that what the LCPC Transform measures is distinct from what volume and surface area measure. Furthermore, while volume and surface area provide only one value for each organoid, the LCPC Transform provides a separate value for each 2D slice of the organoids, each of which can be tracked to its 2D slice. This allows for superior precision in dissecting the components of a 3D object.

The data in Figure 9E match human intuition much better than those in Figure 9F, because these hypothetical organoids were designed to exhibit distinct shapes that are obvious to humans. Organoid 1 is shaped like a pear while Organoid 2 is shaped like a rounded square. The data suggest that the LCPC Transform produces results that are interpretable in ways that volume and surface area are not.

Figure 10A shows the same set of organoids as in Figure 9, while Figure 10B shows a dot plot of the first three principal components of the radial grid LCPC Transform results from these shapes. PCA allows the user to analyze multidimensional data, In Figure 10B, Organoid 2 exhibits compact clustering while Organoid 1 exhibits a broad distribution. This makes intuitive sense because the individual slices of Organoid 2, the rounded square phenotype, are morphologically homogenous. The slices from Organoid 1, on the other hand, exhibit more variation. It makes intuitive sense that slices A, B, and E of Organoid 1 are the furthest away from the rest because their shapes are most distinct out of all the slices of both organoids. Slice C and D of Organoid 1 have a rounded-square morphology like that of Organoid 2 and thus cluster close to the slices of Organoid 2. Slices F, G, and H of Organoid 1 have morphologies like multiple slices in Organoid 2, so it makes sense that they cluster alongside the slices of Organoid 2. Figure 10B is an example of how intuitive the results of the LCPC Transform can be when assessing a 3D object via consecutive 2D slices. This algorithm provides unprecedented precision of 3D objects in ways that area, volume, and surface area cannot.

As explained in the Protocols section, systematically orienting shapes before measuring them with the LCPC Transform yields cleaner data, because nature is inherently polar (i.e. anterior-posterior, apical-basal, etc.). Thus, Figure 10C shows how each slice of the two organoids can be objectively and systematically oriented. In this case, the largest slice of an organoid is identified (Slice D in both) and its longest internal line is determined. This largest slice is then rotated such that the longest internal line becomes vertical. The angle of rotation required to accomplish this is then applied to the rest of the slices of the organoid. Each of the remaining slices of an organoid is rotated according to the same angle that was applied to the largest slice. This is why in Figure 10C the red dotted lines, which are the longest internal lines, do not align perfectly with the dotted green line except for in Slice D. Systematically orienting

the slices in this manner causes shifts in the clustering of the data after performing PCA and plotting the first three principal components in 3D (Figure 10D). The benefits of this systematic orientation before doing the radial grid LCPC Transform are not evident until examining the data in 2D via the first two principal components. Figure 10E shows a much more compact clustering of the slices due to the systematic orientation before doing the LCPC Transform. This enhancement makes data cleaner and thus better for machine learning applications.

For those interested in an example of how organoids can be analyzed as 2D images captured from above, which is the most common way of imaging organoids, a pilot study is described on YouTube (Nguyen, 2025g). This pilot study analyzed a series of brain organoids that exhibited smooth or jagged edges that more accurately quantified by the LCPC Transform than by area.

The same approach applied to individual 2D shapes in Figures 7, 8A, 9, and 10 also apply to the contour of cells in 2D cell culture. The same applies to the shape of cells that are single-cells (such as red blood cells) or as clusters of cells (such as in cervical smears). Pilot studies for each of these cases are described on YouTube:

- Shape analysis of lung alveoli in situ, the same principles can be applied to analyzing 2D cell culture (Nguyen, 2025h).
- Shape analysis of cervical tissue from Pap smears in which both the contour of the nucleus and of the cell membrane are simultaneously quantified via the radial grid LCPC Transform (Nguyen, 2025i).
- Shape analysis of red blood cells infected by malaria and cells adjacent to infected cells but are not themselves infected (Nguyen, 2025j).
- Shape analysis of red blood cels affected by Sickle Cell Disease (Nguyen, 2026).

FIGURE AND TABLE LEGENDS:

Figure 1. Description of the Radial Grid System of the LCPC Transform.
(A) Step 1: The shape of interest is segmented and extracted as a binary mask. Step 2: A bounding box (a.k.a. the smallest rectangle encasing and touching the object on all four sides) is determined for the mask. A system of radial grid lines originating from the center of the bounding box is overlaid onto the mask. The decision to pick the center of the bounding box instead of the centroid of the object as the origin was arbitrary. Step 3: The distance of each intersection between a gridline and the shape is calculated relative to the origin. Grid lines that have more than one intersection sum all those intersection distances into one value for that grid line. Step 4: The FFT is applied to turn the data in Step 3 into a frequency plot, which is a static multidimensional representation (Step 5) of the shape in Step 1. This is similar to how a person's phone number in the USA has nine digits as a static multidimensional representation of their communication line. Step 6: A scalar value can be created from Step 5 via an index. See the "Protocol" section for a discussion on types of indices to calculate. (B) Examples shape themes for which the radial grid system is optimal.

Figure 2. Description of the Parallel Grid System of the LCPC Transform.
(A) Step 1: The shape of interest is manually segmented and extracted as a binary mask. Step 2: A parallel grid system is overlaid onto the shape, which is rotated such that the base is horizontal. Step 3: The distance of each intersection between a gridline and the shape is calculated relative to the baseline. Grid lines that have more than one intersection sum all those intersection distances into one value for that grid line. Step 4: The FFT is applied to turn the data in Step 3 into a frequency plot, which is a static multidimensional representation (Step 5) of the shape in Step 1. This is similar to how a person's phone number in the USA has nine digits as a static multidimensional representation of their communication line. Step 6: A scalar value can be created from Step 5 via an index. See the "Protocol" section for a discussion on types of indices to calculate. (B) Examples shape themes for which the parallel grid system is optimal.

Figure 3. The Importance of Orienting Shapes Systematically for Extracting Clean Data.
(A) An example of identical shapes that are mirror images of each other and how the parallel grid system "sees" their distinct orientation and thus will produce different results. (B) An example of how to flip Shape 2 horizontally, such that it's orientation now matches Shape 1 and result in a fairer comparison to Shape 1. In this configuration, the parallel grid LCPC Transform will yield the same results for both Shape 1 and Shape 2. This alteration of orientation should only be done if there is no spatial context that suggests that Shape 2 should not be modified. (C) An example of four variations of objects that look like the number "3", with some that face the wrong direction. (D) An example of how to orient each object to maximize the cleanliness of the data that will result from the parallel grid LCPC Transform. See the Protocol section for detailed descriptions of the logic behind the orientation rules. (E) An example of measuring the wider bulge of the items in Panel C based on the same orientation rules as for Panel D. (F) An example of measuring the large bulbs of the items in Panel C but keeping their alignment context as in Panel D. The motivation of keeping the alignment rules in Panel D is to dissect the contribution of the spatial information in the wider bulge relative to the contribution of the narrower bulge within these rules.

Figure 4. Measuring Texture-Density with the Parallel Grid LCPC Transform.
(A) Photomicrographs of microvasculature in cardiac tissue reprinted with permission from Gkontra et al. (2018). The two panels on the left are from regions that underwent injury to induce infarction. The two panels on the right are from uninjured regions of the same heart but located remotely from the site of injury. (B) Mask images of the vasculature in Panel A but rotated such that the axis of alignment (green arrows in Panel A) of the vessels is vertical. This objective alignment enhances the cleanliness of the data. (C) The masks from Panel B are cropped to have a circular boundary of uniform diameter, which removes spatial differences due to lost corners when rotating. (D) A plot of the first three principal components of the output from the parallel grid LCPC Transform. (E) Example magnitude values of select bins from the output of the LCPC Transform exhibiting quantitative differences between treatment groups. (F) The percent area of each mask image that is covered by blood vessels.

Figure 5. Hypothetical FFT Results and Common Indices That Can Be Derived From Them.
(A) The profile of two hypothetical shapes is plotted as histograms. Since the magnitudes in Bin 3 and Bin 4 exhibit the opposite trend, a ratio between these two bins will be a good index representing a difference between these two shapes. The red and green dotted lines represent other frequency bins that could be used to derive good indices. (B) A histogram of two hypothetical shapes whose FFT profiles exhibit a stepwise decreasing trend as a representation of their morphological differences. (C) A histogram of two hypothetical shapes whose FFT profiles different most in the central region along the span of frequency bins. (D) Examples of hypothetical indices derived from the same FFT profiles that each represent a distinct morphological feature between the two shapes presented.

Figure 6. The Inability of Traditional Shape Metrics to Register Obvious Context
(A) The series of checkmarks are the same shape but increase in size from left to right. In this series, the area of each checkmark is different while the shape concept remains the same: that is, they remain the same style of checkmarks. (B) A square is rotated about its center for 45-degrees until its shape concept becomes what humans call a diamond. While the shape concept of square is very distinct from that of a diamond, the in-between rotations are subjectively interpreted as either “tilted squares” or “tilted diamonds”. The LCPC Transform can objectively, quantitatively, and robustly measure the different in each step in this series. Note that measures of area and perimeter are unable to describe the changes in this series, because neither change at each step.

Figure 7. Explanation of Pure Shape vs. At-Scale Shape
Measuring objects “At-Scale” means measuring the shape of objects according to their original sizes relatively to each other. “Pure Shape”, on the other hand, means measuring the shape of different objects at a similar scale, which removes the effect of size on the shape. It is important to find on objective manner in which to resize the objects being compared. The longest internal line is an optimal choice (Step 1). Both objects are rotated such that the longest internal line is horizontal (Step 2). In this case, the two objects are also rotate such that the indented side faces down. Next, the width of each object, which is now the same magnitude as the longest internal line of each object, is resized to be 400-pixels wide while also constraining the aspect ratio to prevent skewing the objects (Step 3). Lastly, it is optional to rotate the resized objects 90-degrees before applying the LCPC Transform (Step 4), the rationale about which is discussed in the text.

Figure 8. Example of Spatial Markers for Cancer Research
(A) A hypothetical example of cells migrating in 2D culture by expanding their lamellipodia in the direction of migration. In the context of migratory morphology of epithelial cells, orienting the contour of each cell such that the longest internal line that aligns with the axis of migration is vertical makes the most sense for capturing the spatial context. (B) Hypothetical examples of tumors or pre-cancerous lesions that grow with an encasement that does not change shape. The lesion grows from a stalk, which is the central support structure. As the lesion grows or shrivels, its contour moves towards or away from the internal wall of the encasement. The

dotted lines represent a rational and objective way to define how much of the encasement should be traced (orange line) such that not too little or too much extra information is added. (C) Option 1 shows the parallel grid LCPC Transform applied to the contour of the lesions without context of where the encasement is located. Option 2 shows the same but including spatial context of where the encasement is located.

Figure 9. Novel Quantitation of 3D Organoid Morphology

(A) Two hypothetical organoids separated into consecutive 2D slices. They were designed to look obviously different to humans. Organoid 1 is shaped like a pear while Organoid 2 is shaped like a rounded square. (B) Examples of how the radial grid LCPC Transform identifies the bounding box around each shape and then defines the origin of the radial grid as the center of the bounding box, not the center of the image. (C) Example FFT results for Slice D from each organoid, with the y-axis truncated to better visualize bins with small magnitudes. (D) The value of an index derived as the ratio of the magnitude of Bin 3 divided by the magnitude of Bin 4. The graph shows over a 6-fold decrease between Slice D of Organoid 1 vs. Organoid 2. (E) Box-and-whisker plot of the index values (Bin3/Bin4) of the two organoids. Dotted line encases are enlargement of the Slice A in each organoid, which are the outliers. (F) Traditional measure of volume and surface area as a comparison to the results from the LCPC Transform. The volume and surface area were approximated for Organoid 1 vs. Organoid 2. There is a minor 1.19-fold larger volume in Organoid 2, which is the oppose effect observed in panel E, indicating that the index of Bin3/Bin4 derived from the LCPC Transform measures something distinct from volume. Surface area shows only a 1.002-fold difference, though the general shapes of the two organoids is obviously distinct.

Figure 10. Systematically Orienting Shapes Enhances Cleanliness of Data

(A) 2D slices of hypothetical organoids that were designed to have obviously different shapes. (B) A 3D dot plot of the first three principal component values of each slice of the two organoids in in panel A. Organoid 1 is dark purple while Organoid 2 is yellow. (C) An objective, systematic orientation for each organoid. The longest internal line for Slice D is identified and the whole slice is rotated such that this line aligns perfectly with the vertical axis. Then, the other slices of the same organoid are rotated by the same angle and direction. The red dotted lines (representing the longest internal line) do not align perfectly with the green dotted lines (representing the vertical position) except for in Slice D, because this slice is the reference point for rotating other slices in the same organoid. (D) A 3D dot plot of the first three principal component values of reach slice of the two organoids in panel C. Organoid 1 is dark purple while Organoid 2 is yellow. (E) 2D views of Principal Component 1 (PC1) and Principal Component 2 (PC2) for the radial grid LCPC Transform results of panel A and panel C. Organoid 1 is dark purple while Organoid 2 is yellow. Notice that re-orienting the slices before doing the LCPC Transform results in tighter packing of the clusters (dotted lines), meaning cleaner data.

DISCUSSION:

As with any computational tool, the quality of the output depends on whether the inputs adhere to the expected rules around which the tool was designed. The following rules should be followed and used as quality control checks when utilizing the Python scripts located on the GitHub repositories cited in this study.

1) Do not submit images that have less than 10-pixels of white space on all four sides. See this video for an explanation of why: "The Margin Thickness Parameter - How to Prepare Shape Outlines" (Nguyen, 2025d).
2) This script assumes that the outlines of your object are blue pixels on a white background. The thickness of the line should be between 5-10 pixels thick. See this video for an explanation of why: "The Line Thickness Parameter - How to Prepare Shape Outlines" (Nguyen, 2025e).
3) Do not analyze blank images. This will cause an error in the script.
4) Do not submit images with only a speck of debris. This will cause an error because the grid system may not detect the speck and thus attempt to analyze a blank image.
5) See this video to understand why it is important to understand the scale of your objects before analyzing them with the LCPC Transform: "The Scale Parameter - How to Prepare Shape Outlines" (Nguyen, 2025f).

While the scripts for the LCPC Transform are open-source and thus available for recreation and integration into existing computational pipelines, users who create their own version or modify the preset parameters should check to see if their results match those that are provided as part of this study. The GitHub repositories for the parallel grid and radial grid LCPC Transform scripts contain several sets of practice images and their associated output files. The purpose of including both input and output files is so that users can check to make sure that their version of the script produces identical data as those provided in this study. Most users will adopt the preset parameters in the existing publicly available scripts, so those who alter or integrate the scripts for their own purposes should be aware that their data may no longer match everyone else's.

It is important to note that the results of the LCPC Transform cannot be reconstructed in reverse to derive the original shape of the input object. While the results of the FFT on typical discrete sinusoid data does allow for reconstruction, doing so on FFT data what was obtained on LCPC Transform results does not make sense. Reminder: the LCPC Transform technically finishes before the FFT is applied as a last step, though the phrase "LCPC Transform" in this manuscript is meant to include the FFT as part of the LCPC Transform's routine operation unless specifically stated otherwise.

It is worth adding to the discussion of measuring texture-density relating to Figure 4 in that the human mind is easily confused by optical illusions or disorderly patterns. Haphazard arrangement of complex patterns is often interpreted as being random or not harboring information that is measurable or worth measuring. The LCPC Transform can measure reproducible, objective, quantitative differences in seeming random patterns. However, unless the user is trained to not be fooled by chaotic, disorderly patterns in nature that masquerade as randomness, no attempt will be made to measure the disorder to uncover predictable patterns.

ACKNOWLEDGMENTS:

The author would like to acknowledge Duane Nichols, a high school science teacher who inspired the author to pursue a career in science. Nichols passed away from an aggressive form of colon cancer that kept returning after three surgeries. His passing inspired the author to invent the LCPC Transform to better characterize the morphology of colon polyps. The LCPC Transform is informally referred to as the Nguyen-Nichols Transform to honor the memory of Nichols' impact on thousands of students over many decades. The author would also like to acknowledge Thuan Trinh, his college roommate and friend, who suffered from Bipolar Disorder 2 and took his own life years after college. In desiring to apply the LCPC Transform to the complex morphologies of the human brain in honor of Trinh, the author was inspired to develop ways of enhancing the LCPC Transform, such as adding markers to capture spatial context surrounding the shape of interest. Trinh was an electrical and computer engineer whose discussions with the author at the dining table about the intersection of engineering and biology is part of the inspiration that would one day lead to the author's computational biology research program.

DISCLOSURES:

The author has no conflicts of interest to disclose. The LCPC Transform was commercialized as a software called "Shape Genie" via a company called BrainScanology, Inc., but the patent applications were withdrawn and the company was dissolved.

REFERENCES:

Abbas, Z.N., Al-Saffar, A.Z., Jasim, S.M. et al. Comparative analysis between 2D and 3D colorectal cancer culture models for insights into cellular morphological and transcriptomic variations. *Sci Rep* 13, 18380 (2023). https://doi.org/10.1038/s41598-023-45144-w

Betge, J., Rindtorff, N., Sauer, J. et al. The drug-induced phenotypic landscape of colorectal cancer organoids. *Nat Commun* 13, 3135 (2022). https://doi.org/10.1038/s41467-022-30722-9

Campanale, J. P., Sun, T. Y., & Montell, D. J. Development and dynamics of cell polarity at a glance. *J Cell Sci* 130(7), 1201–1207 (2017). https://doi.org/10.1242/jcs.188599

Ciocalteu, A., Gheonea, D. I., Saftoiu, A., Streba, L., Dragoescu, N. A., & Tenea-Cojan, T. S. Current strategies for malignant pedunculated colorectal polyps. *World J Gastrointest Oncol* 10(12), 465–475 (2018). https://doi.org/10.4251/wjgo.v10.i12.465

Gkontra, P., Norton, K. A., García-Canadilla, P., et al. Deciphering microvascular changes after myocardial infarction through 3D fully automated image analysis. *Scientific Reports* 8, 15841 (2018). https://www.nature.com/articles/s41598-018-19758-4

775 Grimm, D., Corydon, T. J., Sahana, J., González-Torres, L. F., Kraus, A., Marchal, S., Wise, P. M.,
776 Simonsen, U., & Krüger, M. Recent studies of the effects of microgravity on cancer cells and the
777 development of 3D multicellular cancer spheroids. *Stem Cells Transl Med* 14(3) (2025).
778 https://doi.org/10.1093/stcltm/szaf008

779 Hadj Bachir, E., Poiraud, C., Paget, S., Stoup, N., Moghrabi, S. E., Duchêne, B., Jouy, N.,
780 Bongiovanni, A., Tardivel, M., Weiswald, L.-B., Vandepeutte, M., Beugniez, C., Escande, F.,
781 Leteurtre, E., OrgaRES consortium, Poulain, L., Lagadec, C., Pigny, P., Jonckheere, N., Renaud, F.,
782 Truant, S., Van Seuningen, I., & Vincent, A. A new pancreatic adenocarcinoma-derived organoid
783 model of acquired chemoresistance to FOLFIRINOX. *Biology of the Cell* 114, 32–55 (2022).
784 https://doi.org/10.1111/boc.202100003

785 Khune, A. J., et al. Physiological Responses to Space Travel: A Systematic Review. *European*
786 *Journal of Cardiovascular Medicine* 14(5), 450–454 (2024). https://healthcare-
787 bulletin.co.uk/article/physiological-responses-to-space-travel-a-systematic-review-2461/

788 Kim, S. C., Kim, M. J., Park, J. W. et al. Effects of simulated microgravity on colorectal cancer
789 organoids growth and drug response. *Sci Rep* 14, 25526 (2024).
790 https://doi.org/10.1038/s41598-024-76737-8

791 Li, Q., Sun, H., Luo, D. et al. Lnc-RP11-536K7.3/SOX2/HIF-1α signaling axis regulates oxaliplatin
792 resistance in patient-derived colorectal cancer organoids. *J Exp Clin Cancer Res* 40, 348 (2021).
793 https://doi.org/10.1186/s13046-021-02143-x

794 Martin, E., Girardello, R., Dittmar, G., & Ludwig, A. New insights into the organization and
795 regulation of the apical polarity network in mammalian epithelial cells. *FEBS J* 288, 7073–7095
796 (2021). https://doi.org/10.1111/febs.15710

797 Masako Muguruma, Saeko Teraoka, Kana Miyahara, Ai Ueda, Mariko Asaoka, Miki Okazaki,
798 Takahiko Kawate, Masahiko Kuroda, Yohei Miyagi, & Takashi Ishikawa. Differences in drug
799 sensitivity between two-dimensional and three-dimensional culture systems in triple-negative
800 breast cancer cell lines. *Biochemical and Biophysical Research Communications* 533(3), 268–274
801 (2020). https://www.sciencedirect.com/science/article/abs/pii/S0006291X20316727

802 Nguyen, D. H. Translating the architectural complexity of the colon or polyp into a sinusoid
803 wave for classification via the fast Fourier transform [Preprint]. arXiv:1801.06752 [Preprint].
804 2018 Jan 21. Available from: https://arxiv.org/abs/1801.06752
805
806 Nguyen, D. H. Radial-Grid-LCPC-Transform [Internet]. GitHub; 2025 May [cited 2026 Jan 25].
807 Available from: https://github.com/dh2nguyen/Radial-Grid-LCPC-Transform
808
809 Nguyen, D. H. Parallel-Grid-LCPC-Transform [Internet]. GitHub; 2025 May [cited 2026 Jan 25].
810 Available from: https://github.com/dh2nguyen/Parallel-Grid-LCPC-Transform
811

Nguyen, D. H. Pre-Processing-Tools-for-LCPC-Transform [Internet]. GitHub; 2025 May [cited 2026 Jan 25]. Available from: https://github.com/dh2nguyen/Pre-Processing-Tools-for-LCPC-Transform

Nguyen, D. H. The Margin Thickness Parameter - How to Prepare Shape Outlines. YouTube. 2025. Available from: https://youtu.be/byo6Hg6jkiw

Nguyen, D. H. The Line Thickness Parameter - How to Prepare Shape Outlines. YouTube. 2025. Available from: https://youtu.be/pozjMVwsLz4

Nguyen, D. H. The Scale Parameter - How to Prepare Shape Outlines. YouTube. 2025. Available from: https://youtu.be/AIZLg32JgHg

Nguyen, D. H. Shape Genie Quantifies Brain Organoid Morphology in Ways That Area Cannot. YouTube. 2025. Available from: https://youtu.be/_FBtY8a5zmc?si=siT0Lom04dCvBxnM

Nguyen, D. H. Shape Genie Identifies Sub Groups of Lung Alveoli. YouTube. 2025. Available from: https://youtu.be/9c030muLNws?si=T7TJFL23ZQvbd8eU

Nguyen, D. H. Shape Analysis of PAP Smears by Shape Genie. YouTube. 2025. Available from: https://youtu.be/iNcHc2Zb9eM?si=cx67NY3iveNymOID

Nguyen, D. H. Shape Analysis Detects Malaria Without Giemsa Staining. YouTube. 2025. Available from: https://youtu.be/8hCEVxjE_Rg?si=D-XfgsEsAer-R2bK

Nguyen, D. H. Shape Genie Precisely Quantifies Sickle Cell Shapes. YouTube. 2025. Available from: https://youtu.be/E-BfgFHVFl0

Roignot, J., Peng, X., & Mostov, K. Polarity in mammalian epithelial morphogenesis. *Cold Spring Harb Perspect Biol* 5(2), a013789 (2013). https://doi.org/10.1101/cshperspect.a013789

Teo, N. Z., et al. Management of malignant colonic polyps. *Journal of Gastrointestinal Oncology* 11(3) (2020). https://jgo.amegroups.org/article/view/37181/pdf

Tharp, K. M., & Weaver, V. M. Modeling Tissue Polarity in Context. *J Mol Biol* 430(19), 3613–3628 (2018). https://doi.org/10.1016/j.jmb.2018.07.015

Tomsia, M., et al. Long-term space missions' effects on the human organism: what we do know and what requires further research. *Front. Physiol.* 15 (2024). https://doi.org/10.3389/fphys.2024.1284644

Yuan, J., Zhang, S., Xu, Y. et al. Microgravity and cancer cells: from molecular mechanisms to therapeutic strategies. *Cell Death Discov.* 12, 9 (2026). https://doi.org/10.1038/s41420-025-02836-8

851 Zhao, N., Powell, R. T., Yuan, X. et al. Morphological screening of mesenchymal mammary
852 tumor organoids to identify drugs that reverse epithelial–mesenchymal transition. *Nat Commun*
853 12, 4262 (2021). https://doi.org/10.1038/s41467-021-24545-3

854

855

FIGURES

Figure 1

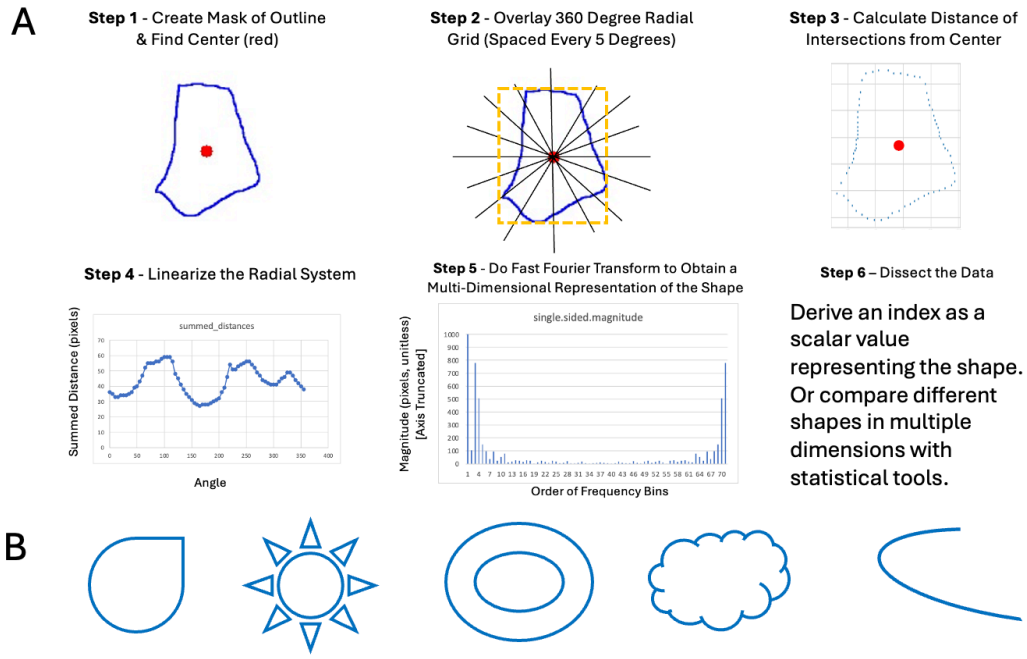

Figure 2

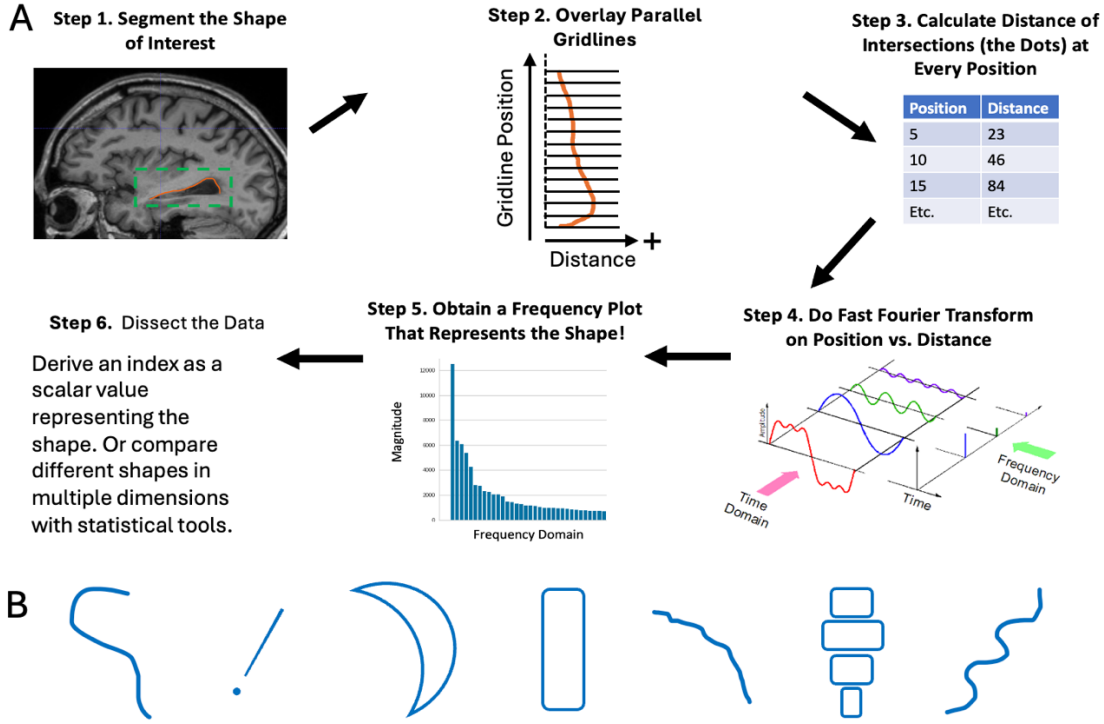

Figure 3

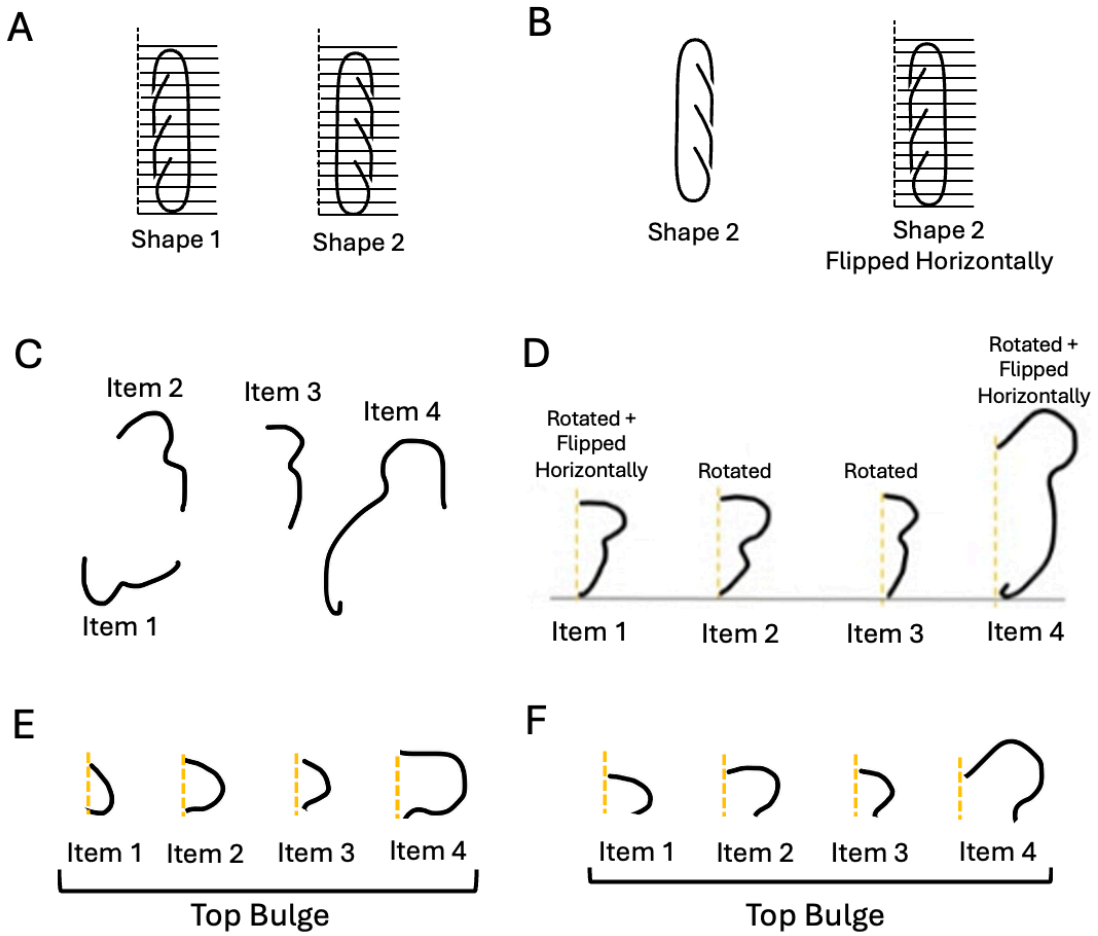
A
Shape 1
Shape 2
B
Shape 2
Shape 2
Flipped Horizontally
C
Item 1
Item 2
Item 3
Item 4
D
Rotated + Flipped Horizontally
Rotated
Rotated
Rotated + Flipped Horizontally
Item 1
Item 2
Item 3
Item 4
E
Item 1
Item 2
Item 3
Item 4
Top Bulge
F
Item 1
Item 2
Item 3
Item 4
Top Bulge

Figure 4.

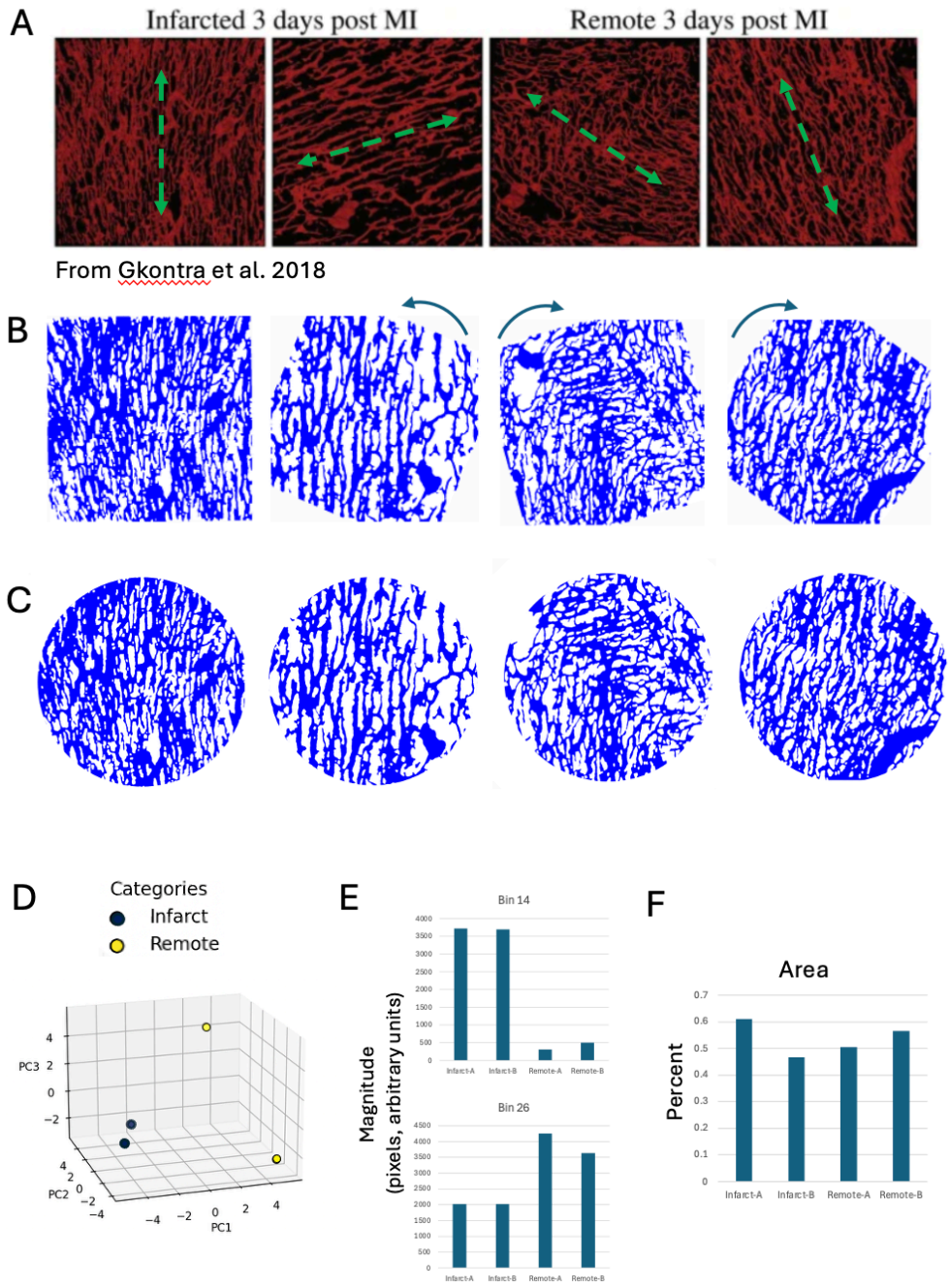
A
Infarcted 3 days post MI
Remote 3 days post MI
From Gkontra et al. 2018
B
C
D
Categories
Infarct
Remote
PC3
PC2
PC1
E
Bin 14
Bin 26
Magnitude
(pixels, arbitrary units)
Infarct-A
Infarct-B
Remote-A
Remote-B
F
Area
Percent

Figure 5

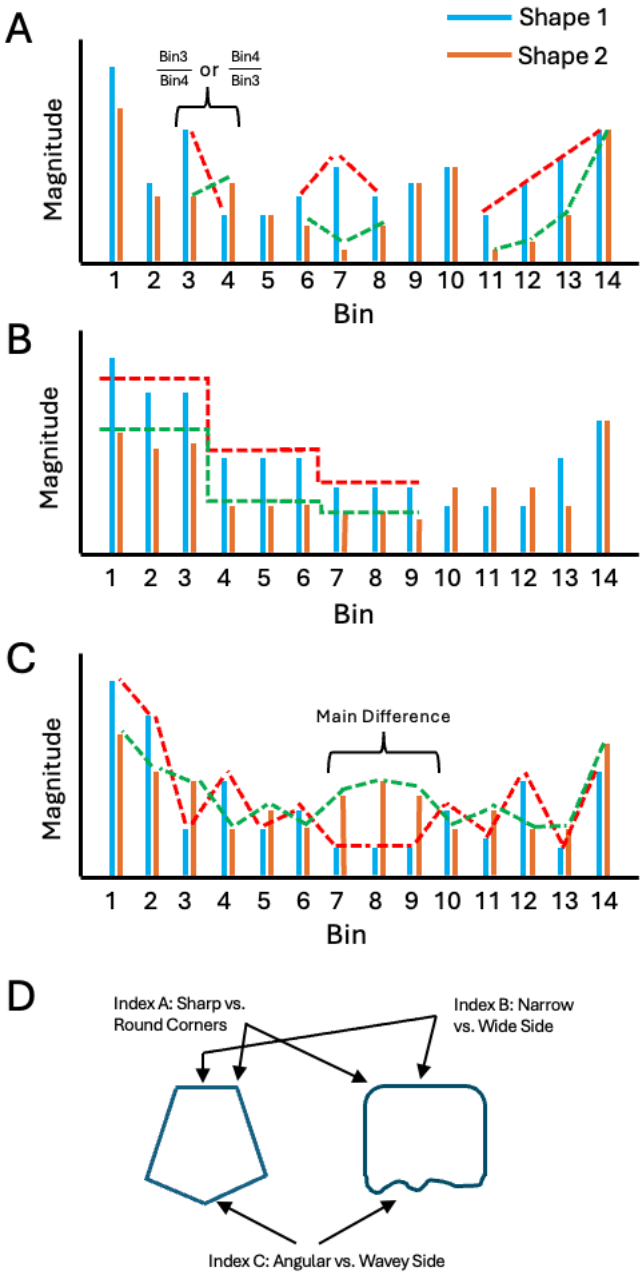
A
Shape 1
Shape 2
Bin3/Bin4 or Bin4/Bin3
Magnitude
1 2 3 4 5 6 7 8 9 10 11 12 13 14
Bin
B
Magnitude
1 2 3 4 5 6 7 8 9 10 11 12 13 14
Bin
C
Main Difference
Magnitude
1 2 3 4 5 6 7 8 9 10 11 12 13 14
Bin
D
Index A: Sharp vs. Round Corners
Index B: Narrow vs. Wide Side
Index C: Angular vs. Wavey Side

Figure 6

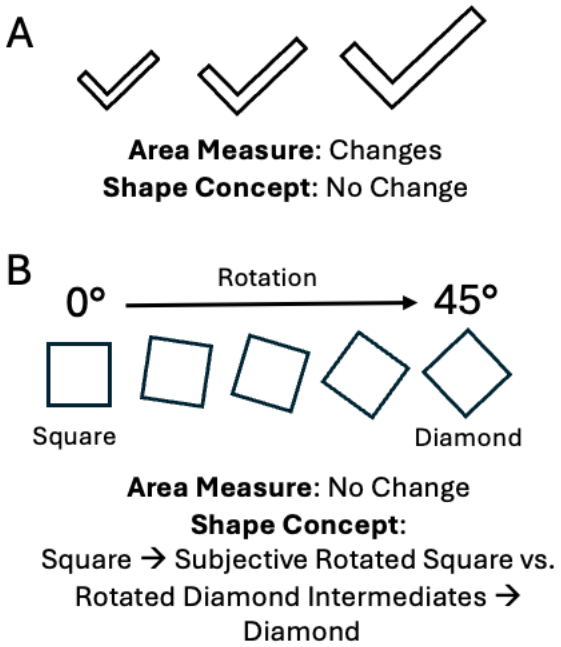

Figure 7

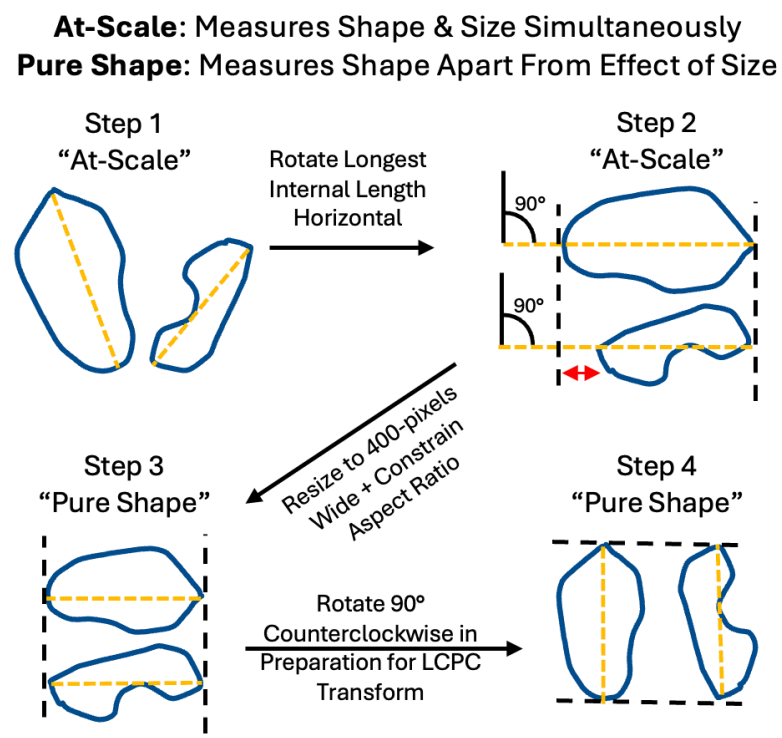

880

Figure 8

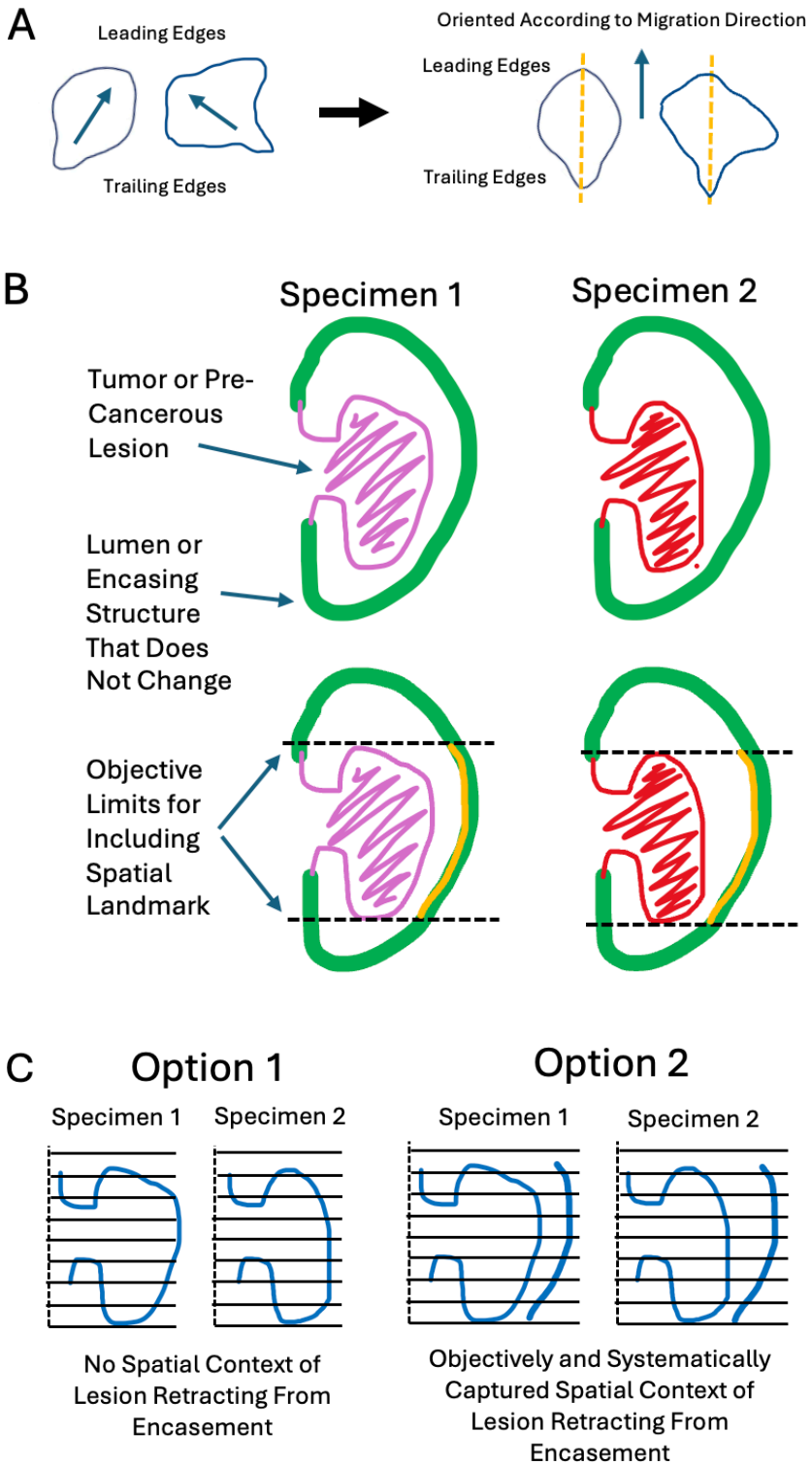

881

882

Figure 9

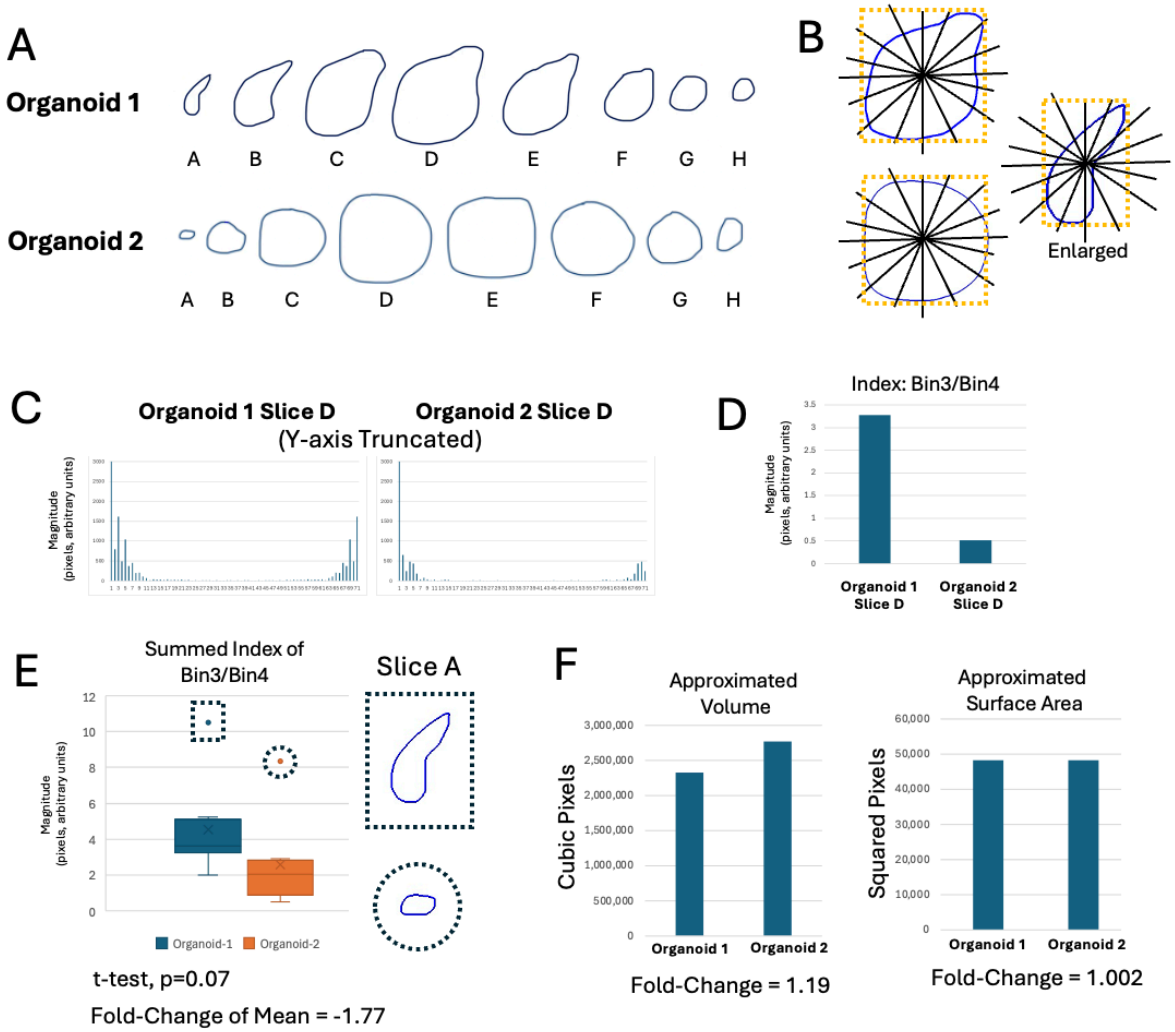
A
Organoid 1
A B C D E F G H
Organoid 2
A B C D E F G H
B
Enlarged
C
Organoid 1 Slice D
Organoid 2 Slice D
(Y-axis Truncated)
Magnitude (pixels, arbitrary units)
D
Index: Bin3/Bin4
Magnitude (pixels, arbitrary units)
Organoid 1 Slice D
Organoid 2 Slice D
E
Summed Index of Bin3/Bin4
Slice A
Magnitude (pixels, arbitrary units)
Organoid-1
Organoid-2
t-test, p=0.07
Fold-Change of Mean = -1.77
F
Approximated Volume
Cubic Pixels
Organoid 1
Organoid 2
Fold-Change = 1.19
Approximated Surface Area
Squared Pixels
Organoid 1
Organoid 2
Fold-Change = 1.002

Figure 10

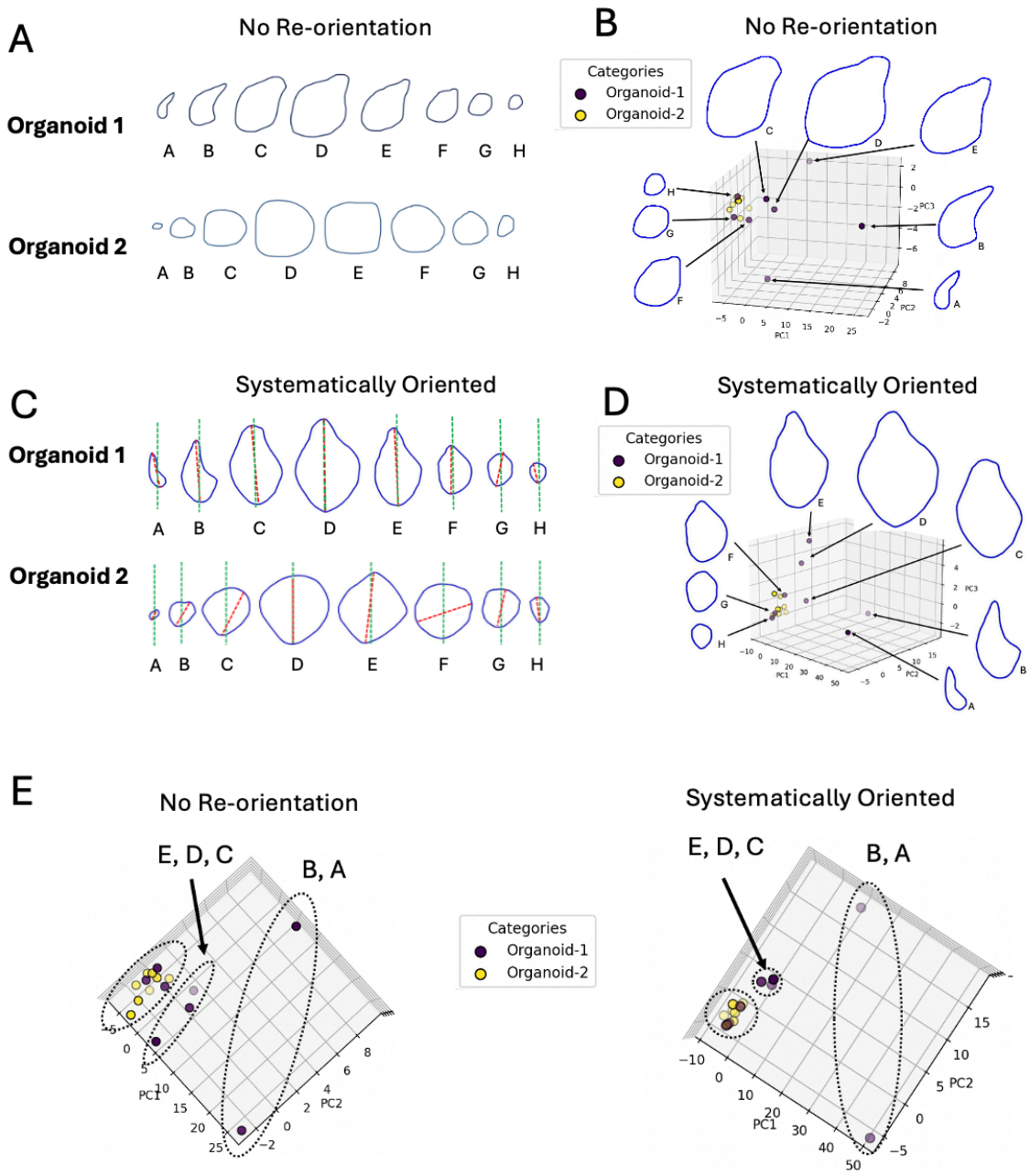

891

892